Plenary: Progress in Regional Landslide Hazard Assessment—Examples from the USA

Rex L. Baum, William H. Schulz, Dianne L. Brien, William J. Burns, Mark E. Reid, and Jonathan W. Godt

Abstract

Landslide hazard assessment at local and regional scales contributes to mitigation of landslides in developing and densely populated areas by providing information for (1) land development and redevelopment plans and regulations, (2) emergency preparedness plans, and (3) economic analysis to (a) set priorities for engineered mitigation projects and (b) define areas of similar levels of hazard for insurance purposes. US Geological Survey (USGS) research on landslide hazard assessment has explored a range of methods that can be used to estimate temporal and spatial landslide potential and probability for various scales and purposes. Cases taken primarily from our work in the U.S. Pacific Northwest illustrate and compare a sampling of methods, approaches, and progress. For example, landform mapping using high-resolution topographic data resulted in identification of about four times more landslides in Seattle, Washington, than previous efforts using aerial photography. Susceptibility classes based on the landforms captured 93 % of all historical landslides (all types) throughout the city. A deterministic model for rainfall infiltration and shallow landslide initiation, TRIGRS, was able to identify locations of 92 % of historical shallow landslides in southwest Seattle. The potentially unstable areas identified by TRIGRS occupied only 26 % of the slope areas steeper than 20°. Addition of an unsaturated infiltration model to TRIGRS expands the applicability of the model to areas of highly permeable soils. Replacement of the single cell, 1D factor of safety with a simple 3D method of columns improves accuracy of factor of safety predictions for both saturated and unsaturated infiltration models. A 3D deterministic model for large, deep landslides, SCOOPS, combined with a three-dimensional model for groundwater flow, successfully predicted instability in steep areas of permeable outwash sand and topographic reentrants. These locations are consistent with locations of large, deep, historically active landslides. For an area in Seattle, a composite of the three maps illustrates how maps produced by different approaches might be combined to assess overall landslide potential. Examples

R.L. Baum (✉) • W.H. Schulz • J.W. Godt
U.S. Geological Survey, Geologic Hazards Science Center, Denver, CO 80225-0046, USA
e-mail: baum@usgs.gov; wschulz@usgs.gov; jgodt@usgs.gov

D.L. Brien • M.E. Reid
U.S. Geological Survey, Volcano Science Center, Menlo Park, CA 94025, USA
e-mail: dbrien@usgs.gov; mreid@usgs.gov

W.J. Burns
Oregon Department of Geology and Mineral Industries, Portland, OR 97232, USA
e-mail: bill.burns@dogami.state.or.us

K. Sassa et al. (eds.), *Landslide Science for a Safer Geoenvironment*, Vol. 1,
DOI 10.1007/978-3-319-04999-1_2, © Springer International Publishing Switzerland 2014

from Oregon, USA, illustrate how landform mapping and deterministic analysis for shallow landslide potential have been adapted into standardized methods for efficiently producing detailed landslide inventory and shallow landslide susceptibility maps that have consistent content and format statewide.

Keywords
Landslide susceptibility • Landslide probability • Deterministic models • LiDAR • Landform mapping

Introduction

Landslides cause untold human misery, with annual fatalities estimated in the thousands worldwide (Kirschbaum et al. 2010; Petley 2012) and annual losses estimated in the billions of dollars (Dai et al. 2002). Efforts to estimate the probability of landslides have resulted in gradual improvements in methods and results over the last five decades. Several authors have published overviews of the state of the art of landslide hazard zonation and related topics at various times (Varnes 1984; Soeters and van Westen 1996; Aleotti and Chowdury 1999; Guzzetti et al. 1999; Dai et al. 2002; van Westen et al. 2006). This paper illustrates our progress on regional landslide hazard assessment during the last decade with selected case studies from work in the U.S Pacific Northwest. We conclude by discussing some of the outstanding issues for ongoing and future research.

Background

Much of the recent progress in landslide hazard assessment has been made possible by recent advancements in technology and availability of digital data. Progress also has resulted from application of scientific advancements in earth science and other fields to landslide problems. After a brief review of the history of landslide hazard assessment, along with a survey of techniques described in the literature, we highlight a few examples of recent progress and developments in regional landslide hazard assessment in the USA. The examples help to illustrate (1) the contributions of recent technological advancements to improved topographic data, (2) the contribution of improved models to analytical results, (3) progress in methods for evaluating or validating model results, and (4) the contribution of standardized methods to rapid production and distribution of landslide maps. This includes mapping in rapid response mode—post-disaster assessments for major landslide events.

Landslide hazard assessment aims to answer questions about where and when landslides will occur, how often they will happen, how large they will be, and how fast and far they will travel. In general, the goal is to assess the (numerical) probability of landslide occurrence or impact (Dai et al. 2002). Regional hazard assessments commonly focus on the questions of location and timing (where and when) with secondary emphasis on frequency (how often), size (how large), and travel distance or inundation area (how far).

The term "regional" has been associated with map scales ranging from 1:100,000–1:500,000 (Soeters and van Westen 1996). For purposes of this paper, we include methods that could be applied at medium scales (1:25,000–100,000) as well, because recent advancements in computer hardware, Geographic Information Systems (GIS), and digital spatial data have made it possible to apply more detailed analysis over larger areas, somewhat reducing the distinction between regional- and medium-scale assessments. Thus, for purposes in this paper, regional refers to methods of landslide hazard assessment that can be applied to areas ranging from tens to thousands of square kilometers.

History

Mapping of landslides and landslide-susceptible areas has been performed since the 1930s or earlier (Varnes 1981). Early efforts were generally local and sporadic. Concerted efforts, mainly by government organizations in various parts of the world, to delineate and zone or rank hazardous areas began to accelerate in the late 1960s. Examples of computer-assisted assessments of landslide hazard began to appear in the early 1970s (Varnes 1984). Most regional landslide hazard assessments published before 1980 were map-based assessments of landslide susceptibility that relied on either cartographic analysis of geology and terrain features or numerical rating of contributing factors (Varnes 1984). Landslide susceptibility usually refers to an assessment of the long-term, qualitative (or relative) probability of landslides, whereas landslide hazard usually refers to a quantitative estimate of probability of landslide occurrence or impact (Soeters and van Westen 1996; Dai et al. 2002).

These studies relied heavily on expert judgment and some combination of field studies and air photo interpretation. For example, in the USA, federal and state agencies developed relative-slope-stability maps at various scales in the 1970s for several major urban areas (Brabb et al. 1972; Miller 1973; Artim 1976). These maps were based on simplified geologic data and topographic slope, generally at scales of 1:30,000–1:125,000, and lacked the currently desired level of detail for managing land use by cities and counties.

By the mid-1990s, improvements in computer hardware and software as well as improvements in satellite remote sensing enabled a number of advancements. GIS methods had advanced to the point that they could be used profitably in analysis of landslide susceptibility and hazard. Concurrently, four distinct, and now commonly recognized approaches for landslide hazard assessment developed: landslide inventory-based probabilistic, statistical, deterministic, and heuristic (Soeters and van Westen 1996). For example, an innovative debris-flow hazard assessment took advantage of GIS technology and statistical methods to calculate debris-flow probability including runout zones (Ellen et al. 1993). Numerous examples of weight of evidence (Harp and Noble 1993; Suzen and Doyuran 2003; van Westen et al. 2003), bivariate (Brabb et al. 1972) and multivariate statistical models (Carrara 1983; Carrara et al. 1991, 1999; Chung et al. 1995) applied to landslide hazard assessment appeared. Satellite remote sensing improved both in terms of spatial resolution and spectral resolution to the point that it could be used to delineate the extent of landslides induced by major regional storms or major earthquakes (Soeters and van Westen 1996). Nevertheless, vertical aerial photography remained the preferred type of imagery for mapping landslides to develop landslide inventories. A number of GIS-based deterministic models (Montgomery and Dietrich 1994; Wu and Sidle 1995; van Westen and Terlien 1996; Borga et al. 1998; Pack et al. 1998) also emerged in the literature. Methods of using landslide inventories to check accuracy of landslide susceptibility and hazard assessments also began to be devised (Carrara et al. 1991; Montgomery et al. 1998). The terms landslide hazard and landslide susceptibility were commonly used interchangeably and despite the technical advances, most maps published by the mid 1990s depicted landslide susceptibility, rather than hazard (Soeters and van Westen 1996).

Steadily increasing numbers of regional- and medium-scale landslide hazard assessments have appeared in the literature since the mid-1990s. Further advancements in science and technology have paved the way for progress in regional landslide hazard assessment in recent years. These advancements include improvements in satellite (InSAR, high-resolution optical) imagery and airborne remote sensing (primarily the airborne laser scanning technology known as Light Detection and Ranging, LiDAR) (Schulz 2004, 2007; Burns and Madin 2009; Roering et al. 2009), as well as platforms for obtaining and visualizing the imagery, such as Google Earth. New methods and existing methods from other fields were applied, such as, artificial neural networks (ANN) (Lee et al. 2003; Lu and Rosenbaum 2003; Falaschi et al. 2009), and logistic regression and other new statistical models (Dai and Lee 2003; Ohlmacher and Davis 2003; Van den Eeckhaut et al. 2006; Felicísimo et al. 2013). Along with these changes have come improvements in methods for validating landslide hazard maps (Chung and Fabbri 2003; Van Den Eeckhaut et al. 2006). Coe et al. (2004a) introduced a method for estimating landslide probability based on historical records. New deterministic models have emerged for assessing large deep landslides (Miller 1995; Reid et al. 2000, 2001, 2010; Franciss 2004; Xie et al. 2004; Brien and Reid 2007, 2008) and shallow rainfall induced landslides (Crosta and Frattini 2003; Savage et al. 2003; Frattini et al. 2004; van Beek and van Asch 2004; Baum et al. 2008, 2010, 2012; Salciarini et al. 2008; Simoni et al. 2008). Technology advances have also made possible more rapid assessments for areas where few data exist (Coe et al. 2004b; Harp et al. 2009). New types of assessments have also been developed, including event–based seismic landslide hazard assessments (Jibson et al. 2000), and post-fire probabilistic debris-flow hazard assessments (Cannon et al. 2010). Models of ground motion are beginning to be applied to analysis of seismic landslides (Harp et al. 2012). Tools originally developed for assessing hazards from volcanic debris flows (Schilling 1998) have been adapted to mapping potential inundation areas for smaller debris flows and rock avalanches (Berti and Simoni 2007; Griswold and Iverson 2008; Magirl et al. 2010).

Throughout the 1990s and before, the main audience for landslide hazard assessments was primarily land-use planners and engineers. Hazard assessments were used so that high-density residential and commercial development or redevelopment of areas with high potential for landslides could be avoided or regulated. More recently, municipal governments and other users have recognized the value of landslide susceptibility and landslide hazard assessments in emergency preparedness planning, landslide early warning, and setting priorities for engineered mitigation of landslide prone-areas (Coe et al. 2004a). Knowing where landslides are likely to occur frequently helps in selecting evacuation routes, placing equipment in preparation for removing debris after a storm, and targeting warnings of potential landslides. Some recent efforts have focused on developing hazard maps for insurance purposes (Godt et al. 2012).

Examples of Progress in Regional Hazard Assessment

As too many examples of recent progress in regional landslide hazard assessment exist in the literature to be cited here, we highlight USGS research that utilized improved spatial data and technology. The improvements in technology have allowed us to develop applications of new statistical methods to landslide susceptibility mapping, improved physically based models, improved methods of evaluation, and standardization of procedures for conducting assessments over large areas or in rapid response mode. In the following sections, we present case studies from our work in the Pacific Northwest of the USA that illustrate progress in some of these areas. Specifically, we present examples of advancements derived from improved spatial data and visualization methods (Schulz 2007), improved deterministic models (Brien and Reid 2007, 2008; Godt et al. 2008a, b; Baum et al. 2010, 2012), improved methods of evaluation (Chung and Fabbri 2003; Van den Eeckhaut et al. 2006), composite hazard assessments, and standardization of methods for rapid assessments (Burns and Madin 2009; Burns et al. 2012).

Seattle Case Study

Baum et al. (2005) described in considerable detail the then ongoing USGS regional assessment of landslide hazard for Seattle, Washington, USA (Fig. 1). In the sections that follow, we highlight some further advancements from that work and combine some of the assessments to illustrate the concept of a composite assessment of landslide potential. Using a common field area, we demonstrate a geomorphic approach based on high-resolution topography and two deterministic methods for separately assessing shallow and deep landslides. The composite integrates results from the three different models to give an overview of the combined potential for all types of landslides that commonly occur in the area.

Geomorphic Assessment of Landslides with LiDAR

The advent of high-resolution remotely sensed topographic data has revolutionized mapping of landslides and landslide features for inventory and susceptibility purposes. As part of our assessment of landslide hazard for the Seattle area, Schulz (2004, 2007) developed and tested a methodology for mapping landslide features using LiDAR data over the entire city of Seattle (217 km^2). These studies used a LiDAR-derived DEM with 1.8 m resolution, and a raw point density of ground returns of about 1 per m^2, with vertical errors of about 30 cm, except in densely vegetated areas, where vertical errors were locally as much as 5 m (Haneberg 2008).

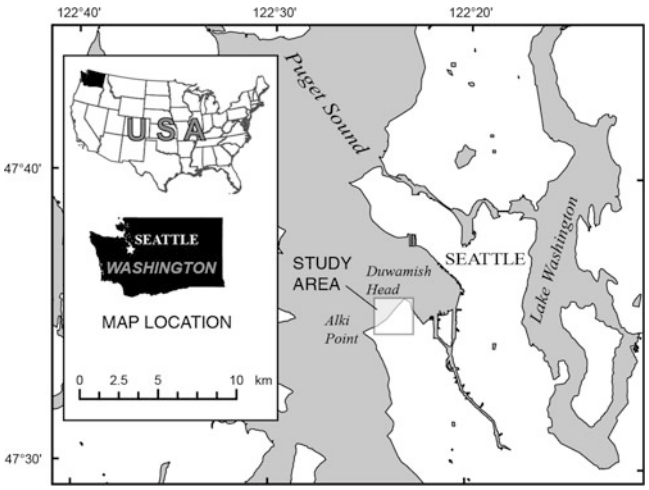

Fig. 1 Map showing Seattle, WA, USA study area

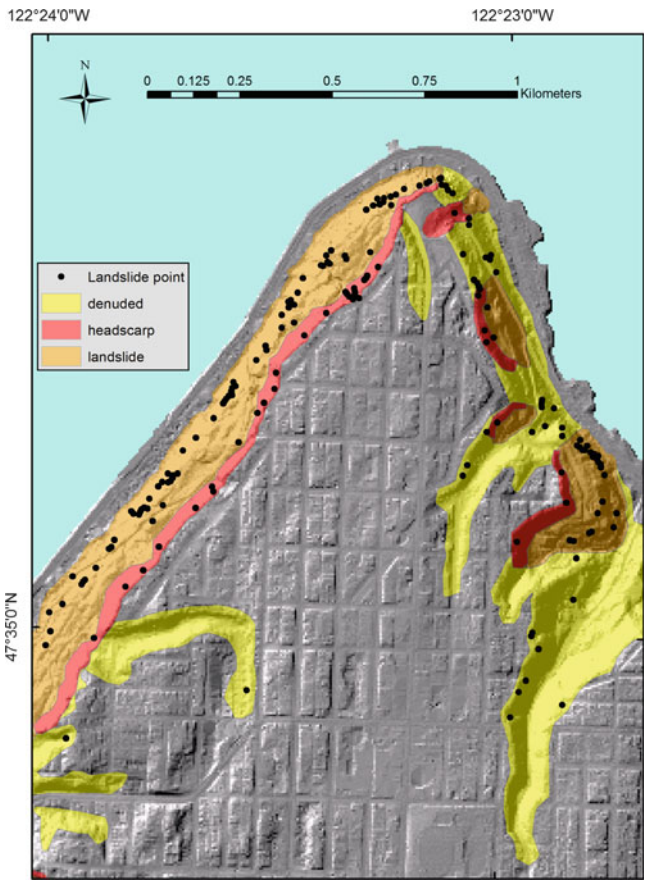

Fig. 2 Map showing landslide-derived landforms identified by Schulz (2004, 2007) using LiDAR imagery for the area shown in Fig. 1

Schulz (2004, 2007) used LiDAR-derived imagery to map landforms in Seattle created mainly by landslide activity. The landforms identified were: (1) landslide deposits, (2) head scarps, and (3) denuded slopes (Fig. 2). These

landforms in all cases truncate the glacially sculpted upland surface. Denuded slopes were defined as slopes that formed by erosion and mass wasting following deglaciation, but which lacked discernible deposits of individual landslides. Denuded slopes, therefore, were mapped where the glacial upland surface is truncated, but where landslides could not be identified. Field observations indicate that denuded slope areas probably lack discernible landslides because many Seattle landslides are too small and thin to be resolved by LiDAR and their deposits have often been removed or modified by erosion, other mass wasting, and human activity.

Using a GIS, landform mapping was performed with LiDAR-derived imagery including shaded relief, slope, and topographic contour maps, as well as almost 400 topographic profiles. These maps and profiles were visually evaluated for topographic characteristics indicative of landslides, such as scarps, hummocky topography, convex and concave slope areas, midslope terraces, and offset drainages. Maps were evaluated at scales ranging from 1:30,000 to 1:2,000; mapping was generally performed at 1:5,000. Mapped landforms were evaluated in the field and the maps were revised based on field observations, although very little revision was necessary.

The total number of landslides mapped using LiDAR was about four times that of previously published maps produced using aerial photographs, and the LiDAR-mapped landslides included all shallow and deep landslides depicted in those maps. In addition, 93 % of historical landslides recorded in the Seattle landslide database (Laprade et al. 2000) are within the boundaries of the LiDAR-mapped landslides. Landslides were consistently identified using the LiDAR imagery if they had landslide-related topographic features that were at least 30 m long and local relief of a few meters. Wait's map (2001) was most applicable for comparison to results of the LiDAR study (Schulz 2004, 2007) and used 1:2,000–1:2,500-scale black-and-white, color, and color-infrared aerial photographs taken during March 1974, June 1986 and 1991, and September 1995 and 1997. Evaluation of Wait's map (2001), which identified the most landslides of previous efforts, indicated that aerial photographs were instrumental for identifying recent individual landslides; therefore, aerial photographs appear to be more effective than LiDAR in the Seattle area for discerning boundaries of recently active landslides within landslide complexes. The resolution of the LiDAR data (1.8 m) appeared to be inadequate to resolve many landslide boundaries within landslide complexes. However, LiDAR was much more effective for identifying presumably older landslides and the boundaries of complexes in which recently active landslides occurred (Schulz 2004).

Schulz (2007) found that historical landslides were concentrated within the mapped landslide-derived landforms, and appeared to generally be located on the steepest parts of slopes. The mapped landforms (landslides, head scarps, and denuded slopes) were created by the temporally integrated influence of many individual landslide events. The landslide, head scarp, and denuded slope landforms cover 4.6 %, 1.2 %, and 9.5 % of Seattle's land area, respectively. The spatial distribution of mapped landforms and 1,308 historical landslides within the Seattle city limits show that historical landslide activity has been concentrated on the mapped landforms, but most of the landslide activity that created the landforms was prehistoric. Thus, the spatial densities of historical landslides within the mapped landforms (122/km^2, head scarps; 42.8/km^2 landslides; 23.7/km^2, denuded slopes), were essentially equivalent to the relative susceptibilities of the landforms to historical and presumably future landsliding. The susceptibilities are relative in that they are only meaningful when compared between landforms or landslides with different characteristics in Seattle.

As with many other landslide inventories, the Seattle landslide inventories constructed using LiDAR, aerial photography, and other means omit many areas prone to landsliding because they exclude excavated landslide scars. Denuded slopes appear to primarily consist of coalescing landslide scars and disrupted, thin landslide deposits. Over 37 % of historical landslides in Seattle occur on LiDAR-mapped denuded slopes, (23 % on head scarps and 33 % on landslides) thus denuded slopes should be considered in regional evaluations of landslide susceptibility even though they have the lowest susceptibility of the three landforms.

By comparing landforms and historical landslide locations with geologic mapping, Schulz (2007) identified no strong relations between stratigraphy and landslide occurrence, regardless of type; however, landslide characteristics and slope morphology appeared to be related to stratigraphic conditions. Human activity was a contributing factor in about 80 % of historical Seattle landslides (Laprade et al. 2000). The distribution of mapped landforms and human-caused landslides suggests the probable characteristics of future human-caused landslides on each of the landforms. The distribution of mapped landforms and historical landslides indicates that erosion of slope-toes by surface water has been a necessary condition for causing Seattle landslides. Through construction of seawalls and related structures, human activity has largely arrested this erosion, which implies that landslide activity will decrease with time as hillsides naturally stabilize. However, landslide activity in Seattle is likely to continue for the foreseeable future.

Assessment of Shallow Landslides Using a Physically Based Model

Godt et al. (2008a) described the results from an application of a distributed, transient infiltration–slope-stability model

for an 18 km^2 area of southwestern Seattle. They used the USGS model TRIGRS: Transient Rainfall Infiltration and Grid-based Regional Slope-stability analysis (Savage et al. 2003; Baum et al. 2008, 2010) that combines an infinite slope-stability calculation with an analytic, one-dimensional solution for pore-pressure diffusion in a soil layer of finite depth in response to time-varying rainfall. The transient solution for pore-pressure response can be superposed on any steady-state groundwater-flow field that is consistent with model assumptions. Applied over digital topography, the model computes a factor of safety, F, for each grid cell at any time during a rainstorm. Input variables may vary from cell to cell, and the rainfall rate can vary in both space and time. For Seattle, topographic slope derived from a LiDAR-based 3-m digital elevation model (resampled from the 1.8-m data) (DEM) and hourly rainfall intensities were used as model inputs. Maps of soil and water-table depths derived from geotechnical borings and a model for observed, systematic variation of colluvium and groundwater depth in relation to specific landforms and the seepage face of the regional aquifer (Schulz et al. 2008) constrained initial and boundary conditions for the model. Material strength and hydraulic properties used in the model were determined from field and laboratory measurements (Godt and McKenna 2008), and a tension-saturated initial condition was assumed. Because the equations of groundwater flow are explicitly solved with respect to time, the results from TRIGRS simulations can be portrayed quantitatively to assess the potential landslide hazard based on changing rainfall conditions.

Factor of safety results (Fig. 3) were evaluated by comparing the locations of 212 historical shallow landslides (a subset of the historical landslide database used by Schulz 2007) with the area mapped as having a factor of safety less than 1.2. An effective landslide hazard map maximizes the number of historical landslide locations included in a hazard class while minimizing the total area mapped in that class (Chung and Fabbri 2003). In a comparison of shallow landslide locations with the results of the hazard map, Godt et al. (2008a) determined that the most susceptible class ($F < 1.0$) includes only 8.4 % of the area steeper than 20° and contains 26 % of the historical landslides. A cutoff of 20° was selected because nearly all historical shallow landslides have occurred on slopes steeper than 20°. For the entire study area, the TRIGRS map captures almost 92 % of the historical landslides but only identifies 26 % of the area with slope angles greater than 20° as potentially unstable during realistic rainfall conditions for Seattle. Effectiveness ratios, defined as the ratio of the percentage of historical landslides to the percentage of the mapped area in each class, range from 3.0 to 7.5, indicating that each class has discriminatory power (Chung and Fabbri 2003). To capture the same

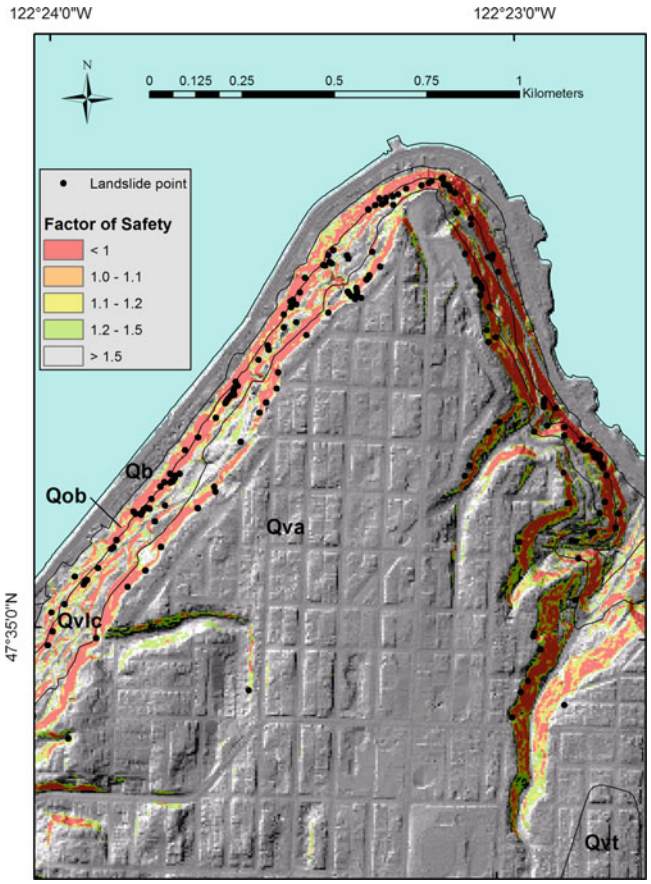

Fig. 3 Map showing part of Godt et al.'s (2008a) factor of safety results for southwest Seattle, computed using the TRIGRS model. *Black points* indicate locations of historical landslides (center of head scarp, Coe et al. 2004a). The predicted factor of safety is at the end of a simulation of a 28-h rainfall event (17–18 January 1986) that induced many shallow landslides. This simulation used the saturated, finite-depth infiltration solution (Savage et al. 2003; Baum et al. 2008, 2010) and is based on Fig. 14 of Godt et al. (2008a). Geologic contacts are shown as gray lines. Interpretations of geologic unit symbols are Qb—beach deposits, Qvt—Vashon till, Qva—advance outwash deposits of the Vashon Drift, Qvlc—Lawton Clay Member of the Vashon Drift, Qob—Olympia beds (interbedded sand, clayey silt and silty clay)

percentage of historical landslides (92 %) using only topographic slope would require all areas with slope angles greater than 20° to be considered susceptible. Thus, the main discriminatory power of the model, as applied in southwestern Seattle, is its ability to exclude nonsusceptible steep (>20°) hillslope areas from the susceptible classes. This is the result of both the spatially variable input (colluvium thickness and initial water-table depth) and the modeling approach.

Recent advancements with the TRIGRS model include an unsaturated infiltration module (Savage et al. 2004; Baum et al. 2008, 2010), a module for analyzing 3D slope stability (Baum et al. 2012), and progress on methods for specifying

model parameters using sensitivity analyses (Gioia et al. 2013) and using a probabilistic framework (Raia et al. 2013). Figure 4 compares results for the Mukilteo study area north of Seattle using the original 1D saturated infiltration model, the 1D unsaturated infiltration module, and the saturated and unsaturated infiltration models combined with a simple method of columns for 3D slope stability. Landslide polygons depicted in Fig. 4 include the source area and deposit of each shallow landslide that occurred during the winter of 1996–1997 and provide a more complete indication of unstable areas for comparing model results than the landslide points available for southwest Seattle (Fig. 3). Analysis using the Receiver Operating Characteristics (ROC) analysis (Swets 1988; Fawcett 2006), which recently has become widely used (Van den Eeckhaut et al. 2006; Falaschi et al. 2009), indicates lower false positive rates achieved by the 1D unsaturated model compared to the 1D saturated, and improvements of the simple 3D analysis compared to the 1D infinite-slope analysis (greater true positive rate with slight or no reduction in false positive rate). In the case shown, the 3D saturated model predicts a greater fraction of the historical landslides than the unsaturated model, at the expense of higher rate of false positives.

Assessment of Large Landslides with the 3D Slope-Stability Model, SCOOPS

In Seattle, deep-seated landslides on bluffs along Puget Sound have historically caused extensive damage to land and structures. These large landslides are controlled by three-dimensional (3D) variations in material strength and pore-water pressures. The 3D effects of groundwater, geology, and landslide geometry greatly complicate analysis of large, deep landslides when compared to small, shallow slides. Although the infinite slope analysis has been applied successfully to shallow landslides, especially where the landslides are close to the size of the DEM grid cells, infinite slope analysis is generally inadequate for large deep landslides. USGS researchers have developed a computer program, SCOOPS (Reid et al. 2000), to assess the slope stability of a digital landscape, as represented by a DEM. SCOOPS has been used to assess the relative stability of volcanic edifices (Reid et al. 2000, 2001, 2010) as well as other settings where large landslides might occur (Brien and Reid 2007, 2008). SCOOPS calculates slope stability by extending conventional two-dimensional (2D) limit-equilibrium analysis to three dimensions (3D) using a method of columns. SCOOPS systematically searches a digital landscape and computes the stability of millions of potential landslides encompassing a wide range of depths and volumes that potentially affect different parts of the DEM, thereby allowing determination of the minimum factor of safety at each DEM cell.

Brien and Reid (2007, 2008) assessed the slope stability of part of southwestern Seattle using SCOOPS coupled with a 3D groundwater flow model (MODFLOW-2000, Harbaugh et al. 2000). The availability of high- (3-m-) resolution digital topography, detailed geologic mapping (1: 12,000 scale, Troost et al. 2005), and a compilation of subsurface exploration logs were used to build 3D models of geology, groundwater, and slope stability. In order to assess the relative stability of coastal bluffs for potential large deep-seated landslides, digital topography (represented by a DEM) was combined with 3D interpretations of geologic mapping and published strength values for the geologic units. The 3D geologic model (Fig. 5) consists of four layers derived from the mapped geologic units. The influence of 3D pore pressures was incorporated based on the results of a 3D groundwater flow model using MODFLOW-2000, calibrated with measured groundwater levels.

The geology of the Seattle area consists of a layer of permeable glacial outwash sand overlying less permeable glacial lacustrine silty clay (Troost et al. 2005). Incorporation of these layers as hydrogeologic units in a 3D groundwater model reproduced an elevated water table above the less permeable units. This water table produces elevated pore pressures in the uppermost hydrogeologic unit, hence a destabilizing factor. The simulated 3D pore-pressure distribution from average rainy season and extreme rainy season recharge scenarios were then used to quantify the stability of the coastal bluffs in SCOOPS. Figure 6 shows factor of safety results for three potential scenarios: (a) moderately large potential landslides (3,000–30,000 m^3) with average rainy season recharge, (b) moderately large potential landslides with extreme rainy season recharge, and (c) very large potential landslides (30,000–300,000 m^3) with extreme rainy season recharge. The analyses indicate that the least stable areas (low values of F, Fig. 6) are steep portions of the uppermost geologic unit, a permeable sand (Qva, see Fig. 5). The elevated pore pressures in this geologic unit produce a destabilizing factor and low factors of safety compared to steep areas in other geologic units. This result is consistent with historical observations of the location of deep-seated landslides. Regions predicted to be least stable include the areas in or adjacent to three mapped historically active deep-seated landslides. Groundwater flow also converges in coastal reentrants, resulting in elevated pore pressures and destabilization of slopes in reentrant regions. As expected, areas of low factor of safety expand with extreme rainy season conditions. Factor of safety greatly decreases in the topographic re-entrants where groundwater flow is concentrated due to topographic convergence. The results of the 3D analyses differ significantly from a slope map or results from one-dimensional (1D) analyses of shallow landslide potential (Fig. 3).

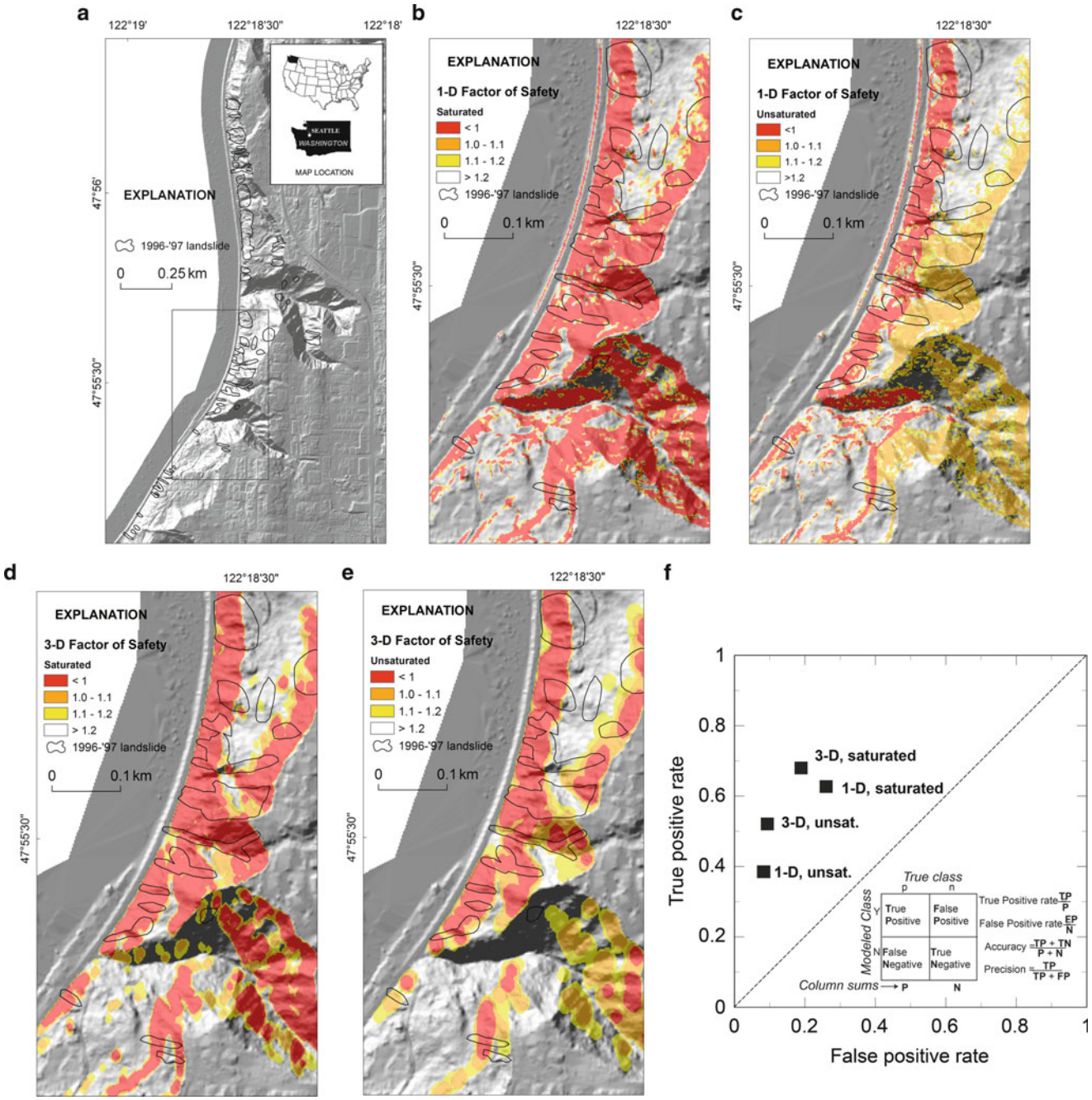

Fig. 4 Maps and diagrams showing factor of safety computed using the TRIGRS model for the Mukilteo study area, about 15 km north of Seattle. (**a**) Location and outlines (scarp and deposit) of 1996–1997 shallow landslides. *Rectangle* indicates area shown in (**b**–**e**). Factor of safety results for (**b**) saturated infiltration and 1D infinite-slope analysis (Godt et al. 2008b), (**c**) unsaturated infiltration and 1D infinite-slope analysis (Baum et al. 2010), (**d**) saturated infiltration and simplified 3D limit-equilibrium slope stability analysis, (**e**) unsaturated infiltration and simplified 3D limit-equilibrium slope stability analysis (Baum et al. 2012) are (**f**) compared for performance using a Receiver-Operating Characteristics (ROC) plot. A perfect prediction would plot at the *upper left corner* of the ROC plot

Composite Landslide Assessment

One of the advantages of using different approaches to assess landslide hazard is the ability to make a composite map showing all hazardous areas identified by the different approaches. A composite or ensemble map can reduce the uncertainty about where landslides might happen by combining the results of different analyses that address the potential for specific types of landslides. Some technical challenges exist in combining the results of different mapping approaches to create a defensible composite (i.e.,

a map created using an objective, reproducible, and quantitatively rigorous method). To combine the two factor of safety maps, (Figs. 3 and 6), which have continuous values, with the geomorphologically based map of landslide-derived landforms, (Fig. 2), we arbitrarily assigned factor of safety values to each landform type (head scarps, 0.99; landslide deposits, 1.099; and denuded slopes, 1.199) based on relative density of historical landslides in each. We then assigned the lowest factor of safety (corresponding to the highest susceptibility) among the three input maps to the composite map.

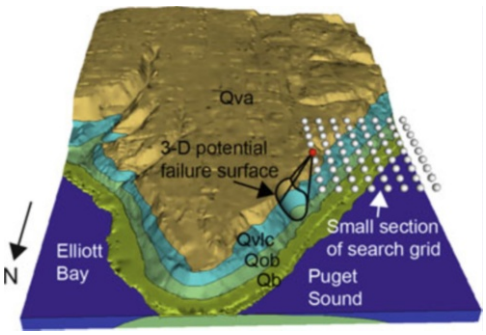

Fig. 5 Perspective view, looking south, of the topography in the southwestern Seattle study area (Fig. 1) with an example of a potential failure removed. The view shows the 3D geologic model, and one layer of a small section of a coarse-resolution search grid used in SCOOPS. Geology is a 3D interpretation (Brien and Reid 2007, 2008) of the geologic map by Troost et al. (2005). Topography is from the City of Seattle 3-m DEM (2000, written commun.) (after Brien and Reid 2008, Fig. 5). Interpretations of geologic unit symbols are Qb—beach deposits, Qvt—Vashon till, Qva—advance outwash deposits of the Vashon Drift, Qvlc—Lawton Clay Member of the Vashon Drift, Qob—Olympia beds (interbedded sand, clayey silt and silty clay)

Figure 7 shows a composite map that combines the areas identified by the geomorphological approach (Schulz 2007), the analysis for shallow landslide potential (Godt et al. 2008a), and the analysis for deep landslide potential (Brien and Reid 2008). This map displays the highest susceptibility level identified at each grid cell by the component maps to show the "worst" case. Whereas the map includes many areas that would be included on a slope map, it also includes some susceptible areas of low slope and areas of medium landslide susceptibility are quite different than would be predicted based on slope alone. Such a map can be used as an initial screening tool to identify areas that have high, moderate, or low composite landslide potential, without being specific about the particular landslide type. This assumes that the high, moderate, and low potential areas on the three component maps are equivalent. Equivalent classes might be established, for example, by setting the boundaries for high, medium, and low on the factor of safety maps equal to densities of corresponding landslide types on the landform map.

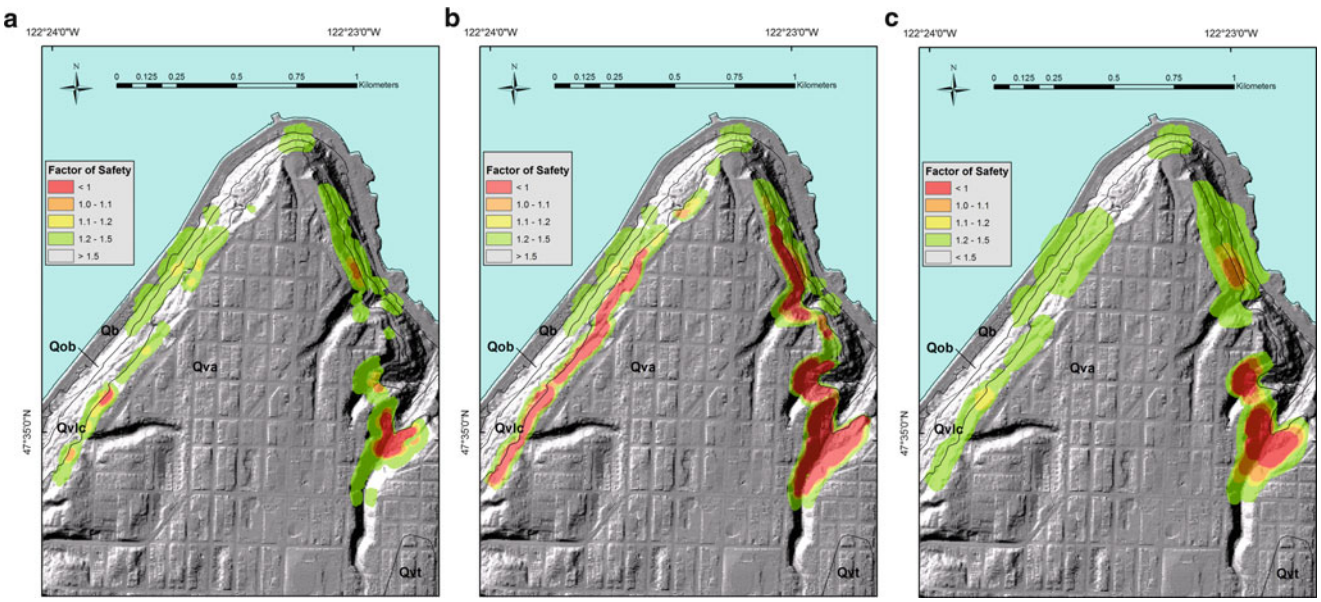

Fig. 6 Map images showing factor of safety (F), computed using the slope-stability model SCOOPS, for 3D critical surfaces with associated volumes between 3,000 and 300,000 m^3. A critical surface is the potential failure with the lowest F at each digital elevation model cell. F is indicated by color. Results are shown for (**a**) moderately large potential landslides (3,000–30,000 m^3) with average rainy season recharge, and (**b**) moderately large potential landslides with extreme rainy season recharge, and (**c**) very large potential landslides (30,000–300,000 m^3) with extreme rainy season recharge. Geologic contacts are shown as *gray lines*. Interpretations of geologic unit symbols are Qb—beach deposits, Qvt—Vashon till, Qva—advance outwash deposits of the Vashon Drift, Qvlc—Lawton Clay Member of the Vashon Drift, Qob—Olympia beds (interbedded sand, clayey silt and silty clay) [modified from Brien and Reid (2008), Fig. 8]

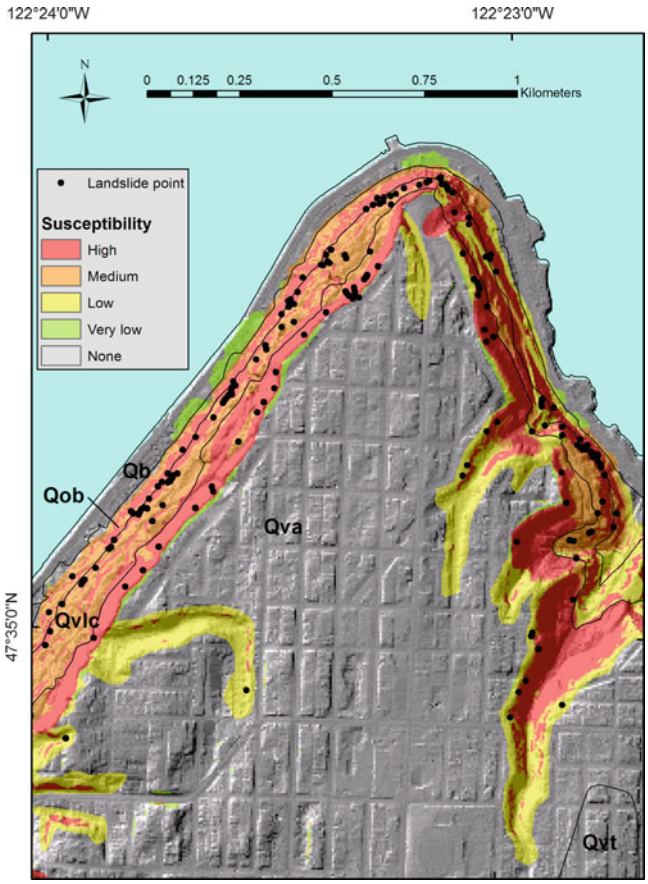

Fig. 7 Composite landslide susceptibility map showing worst susceptibility class (high, medium, low) for each pixel based on results shown in Figs. 2, 3, and 6b. Geologic contacts are shown as gray lines. Interpretations of geologic unit symbols are Qb—beach deposits, Qvt—Vashon till, Qva—advance outwash deposits of the Vashon Drift, Qvlc—Lawton Clay Member of the Vashon Drift, Qob—Olympia beds (interbedded sand, clayey silt and silty clay)

Relating the landforms and the factor of safety to historical landslide density might allow a more rigorous assignment of factor of safety to the landforms. We did not attempt this for the map shown in Fig. 7, due to the different extent of areas considered in each analysis. Taking this idea a step further, the landslide density could be used to estimate landslide probability by adding a temporal frequency corresponding to computed values of factor of safety for shallow (Fig. 3) and deep landslides (Fig. 6) respectively and within each landform type (Fig. 2). A composite map depicting maximum landslide probability drawn from the three analyses (shallow landslides, deep landslides, and landslide landforms) would present a somewhat different picture than Fig. 7, because it would explicitly consider the lower frequency of large, deep landslides. In other words, the weight given to each of the three maps in defining the composite would be different.

Standardized Methods and Rapid Assessments

Improvements in technology for remote sensing, increasingly rapid dissemination of remotely sensed spatial data, and GIS have made it possible to standardize methods for rapidly conducting regional landslide hazard assessments. For example, Cannon et al. (2010) developed tools for assessing the potential for debris flows in previously burned areas. These assessments can be completed in a matter of days after containment of a wildfire. Similarly, Harp et al. (2009) devised methods for rapidly assessing potential for future precipitation-induced landslides after a major storm. Their method makes use of a landslide inventory for a single event (i.e., the major storm) to calibrate a factor of safety model; this has been accomplished even in developing areas (Honduras, Micronesia) where few or no geotechnical data are available. In 2005, the Oregon Department of Geology and Mineral Industries (DOGAMI) began a collaborative landslide research program with the USGS Landslide Hazards Program to identify and understand landslide hazards in Oregon, USA. A major result of this collaboration has been development of standard procedures (protocols) for landslide mapping and susceptibility analysis. These procedures made it possible to map large areas in Oregon uniformly.

Oregon Landslide Mapping Protocol

Landslides are one of the most widespread, frequent, and damaging natural hazards in the state of Oregon (Burns and Madin 2009). To create a consistent landslide inventory for Oregon as a starting point for assessing landslide hazard, DOGAMI developed a protocol for mapping recent and prehistoric landslides using LiDAR imagery (Burns and Madin 2009). Encouraged by the findings of Schulz (2004, 2007), a pilot project area was selected in western Oregon to compare remote sensing data/images for effectiveness (Burns 2007). Data considered in the study included 30-m SRTM, 10-m USGS DEM, 7-m City of Portland DEM, 1-m LiDAR DEM, and stereo color aerial photography. Two key findings from this pilot study were: the use of 1-m LiDAR data (1) resulted in identification of 3–200 times the number of landslides found with the other data sets, consistent with findings in Seattle (Schulz 2004, 2007), and (2) greatly improved the accuracy of the spatial extent of the landslides thus identified. Consequently, LiDAR-derived digital elevation models were selected as the base from which to create the landslide inventories throughout Oregon. The inventory includes all landslides, distinguished by type and recency, that can be identified using the LiDAR imagery, as well as any landslides known from previous inventories. Creating the protocol and its associated map template and geodatabase has somewhat streamlined mapping and publication of landslide inventory data. Following a standard

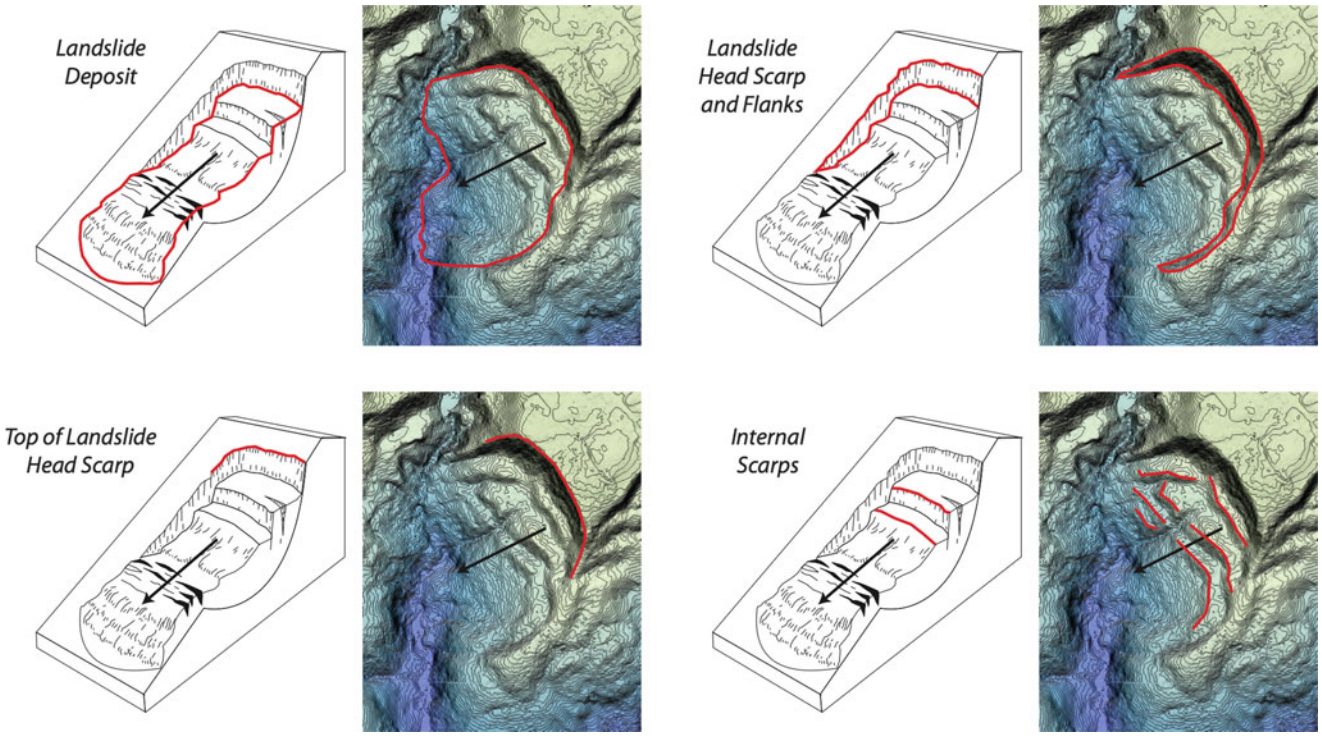

Fig. 8 *Block diagrams* and *map views* showing the four kinds of landslide features that are routinely identified and mapped using the Oregon landslide mapping protocol [after Burns and Madin (2009), Fig. 12]

procedure reduces time required to map the landslides and record the attributes by eliminating the need for the mapper to experiment with visualization techniques or decide what attributes to map. Nevertheless, successful adaptation of the protocol requires a mapper with a reasonable level of expertise on the topic and time to represent all the features. Using the map template and referencing the protocol (Burns and Madin 2009) similarly simplifies the effort needed to prepare the map for publication.

The inventory mapping protocol prescribes procedures for base data acquisition and visualization, mapping landslide features and recording attributes in GIS, field checking, a map template for displaying results, and outlines limitations and recommended use of the landslide inventory data produced by the process (Burns and Madin 2009). The method relies on use of several types of base data: a 1-m DEM derived from LiDAR data with point density averaging 1 m^{-2} or better, a slope map derived from LiDAR data, orthorectified aerial photo of similar age to the LiDAR data, previous landslide inventories or other data on landslides within the proposed mapping area, and a geologic map. Through trial and error, Burns and Madin (2009) determined optimal procedures for visualizing the data to accurately identify landslides and map landslide features, such as, head scarps and internal scarps (Fig. 8). These features are useful in assessing confidence of landslide identification, and scarp height is useful in estimating minimum landslide depth. They also developed a geodatabase template for acquiring landslide attribute data, including classification, dimensions and other quantitative data, confidence of interpretation, and geologic unit. Thus, the protocol includes not only recommended procedures for mapping landslides using LiDAR data, but also specific guidance on setting up the GIS geodatabase necessary for mapping and recording tabular data about each landslide. The final product is a map and database of landslide deposits and features at a scale of 1:8,000, tiled by quarters of USGS 7.5-min quadrangles (Fig. 9).

Oregon Shallow Landslide Susceptibility Protocol

In addition to the landslide inventory mapping protocol, DOGAMI developed a standardized procedure for developing shallow-landslide susceptibility maps. The shallow-landslide susceptibility map protocol combines an inventory of existing landslides, as described previously (Burns and Madin 2009) with hazard zones derived from a Factor of Safety map and buffers (Burns et al. 2012). This protocol also includes a map template for producing a standardized shallow-landslide susceptibility map at a scale of 1:8,000. For purposes of this protocol, DOGAMI defined 4.6 m as the depth boundary between shallow and deep landslides. Like the protocol for mapping landslides described in previous paragraphs, the protocol includes not only recommended procedures for mapping susceptibility to shallow landslides

Fig. 9 Image showing a segment of a landslide inventory map using Oregon's landslide mapping protocol [modified from Burns and Madin (2009), Fig. 24]. Color and symbol designations follow: active or historical landslides, *red*; prehistoric landslides, *yellow*; head scarps, *gold*; shallow, *solid color*; deep, stippled; *RS-R* rock slide-rotational, *RS-T* rock slide-translational, *EFL* earth flow, *ES-R* earth slide-rotational, *ES-T* earth slide translational, *DF* debris flow

using LiDAR data, but also specific guidance on setting up the GIS geodatabase necessary for doing the analysis.

The protocol includes several steps. First, all shallow-seated landslide deposit polygons (except channelized debris-flow deposits, i.e., fans) and their head-scarp polygons are queried from the inventory database (described above) and converted to a raster map with the polygons assigned to the high-susceptibility zone. The backbone of the procedure is the factor of safety computation. As with most other shallow-landslide susceptibility analyses, the factor of safety is computed using a 1D, cell-by-cell infinite-slope analysis (Montgomery and Dietrich 1994; Pack et al. 1998). Specifically, the factor of safety is computed using the same formula as Harp et al. (2006, 2008). Burns et al. (2012) provide suggested values of geotechnical parameters for geologic units common throughout western Oregon. To simplify the GIS analysis, the factor of safety is computed in a spreadsheet to determine threshold slope values based on engineering practice as described by Burns et al. (2012) for high ($F < 1.25$), medium ($1.25 \leq F \leq 1.5$), and low susceptibility ($F > 1.5$) categories (Table 1). Once the factor of safety categories have been applied to the LiDAR-derived slope map, the factor of safety map is filtered (or "clipped") to remove low factor of safety artifacts of low retaining walls and other fine-scale topographic features. Filtering is accomplished using local relief of less than 1.2 m within 4.6 m horizontally of each grid cell. Clipping areas out of the factor of safety map that have low values of local relief removes (1) flat areas, (2) areas with continuous but gentle slopes, or (3) areas with steep slopes but low relief, such as, a near-vertical step. Case 1 has no net effect on the map; case 2 limits the amount of relief, and case 3 is the objective of filtering. Using 1.2 m of local relief over 4.6 m limits the filtering in areas of continuous slope (case 2) to slopes less than 15°. Buffers are then applied to account for potential instability in the (1) areas directly upslope from landslide scarps and (2) areas of low or moderate factor of safety ($F < 1.5$, Table 1, Fig. 10). The head scarp buffer is a 9.2-m-wide (twice the 4.6-m maximum depth) buffer applied to the upslope side of all the shallow landslide head-scarp polygons. A similar 9.2-m-wide buffer is also applied along the upslope edge of all areas having $F < 1.5$ (Table 1, Fig. 10). The final susceptibility map is a composite of the areas of shallow landslide deposits and scarps, the filtered factor of safety zone map, and the buffers (Table 1). A map publication template, similar to the one used for the inventory map, provides for expeditious dissemination of the finished map.

Table 1 Summary of factors contributing to the final shallow-landslide susceptibility map

Contributing factors	Susceptibility zones		
	High	Medium	Low
Factor of safety (*F*)	<1.25	1.25–1.5	>1.5
Landslide deposits and head scarps	Included	–	–
Buffers	2H:1V head scarps	2H:1V $F < 1.5$	–

Discussion and Conclusion

Since the early days of landslide hazard assessment, one of the major issues has been and continues to be data uncertainty. Hazard and susceptibility maps can commonly identify a major fraction of the area subject to landslides, but a remaining smaller fraction remains very difficult to identify (van Westen et al. 2006). This results in large part from the difficulty in quantifying subsurface factors such as groundwater flow patterns, the spatial distributions of colluvium thickness, physical properties, discontinuities

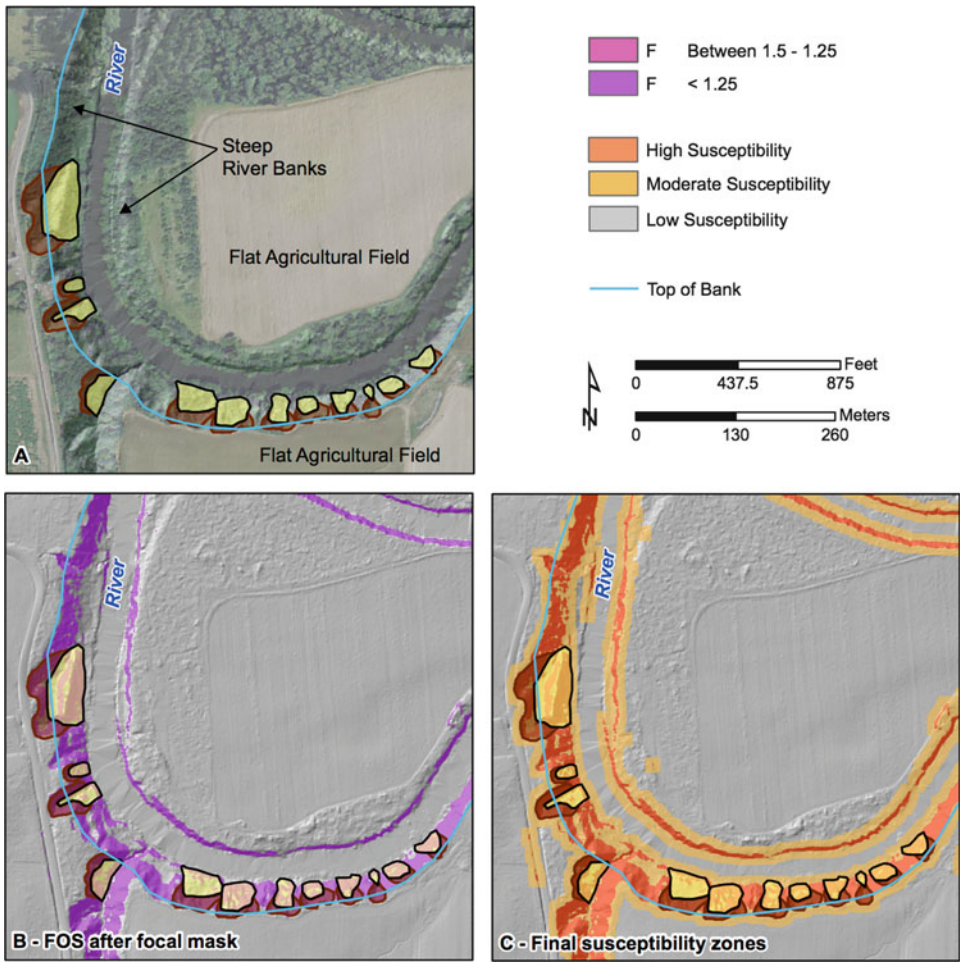

Fig. 10 Sample maps illustrating head-scarp and Factor of Safety, *F*, buffer components (Table 1) of Oregon's shallow landslide susceptibility protocol. (**a**) Landslide inventory (landslide deposits shown as *yellow* polygons and head scarps shown as *red* polygons) displaying the top of head scarps above the top of the locally steep slope (riverbank) area. (**b**) *F* zone map filtered to remove artifacts from low-relief features. (**c**) Filtered *F* zone map with head scarp and *F* buffers added [modified from Burns et al. (2012), Fig. 21]

and other properties of the subsurface that affect slope stability. Surrogates for these factors, such as geological or soils map units, vegetation type, and others too numerous to list, that are commonly used in statistically based regional assessments are likewise subject to uncertainty due to transitional or obscure contacts, with unknown subsurface geometry, and sometimes subtle or subjective differences between map units. Effects of land use and land-use changes, as well as temporal climate variability, likewise introduce uncertainty into hazard assessments. As a result of these sources of uncertainty, probabilistic frameworks are commonly needed to couch the results of hazard assessments. Regardless of expected advances in probabilistic analysis, which will surely help, major future progress in landslide hazard assessment will in large measure depend on progress in reducing data uncertainty.

Despite the difficulties imposed by data uncertainty, technological advancements have enabled significant progress. High-resolution topographic data, particularly when used in combination with high-resolution optical imagery, can contribute to greatly improved mapping and identification of landslide deposits and features as demonstrated by recent work (Schulz 2004, 2007; Burns 2007; Burns and Madin 2009; Roering et al. 2009). This is encouraging because high-quality landslide inventories are the backbone of regional and medium-scale landslide hazard assessments (Harp et al. 2011) and besides topography and optical imagery, few other data that are needed to specify landslide susceptibility or slope stability model parameters exist in many areas of the world.

Improvements to deterministic models, such as those demonstrated here, are contributing to progress in

regional landslide hazard assessment by making better use of those data that are available and making better estimates of potential landslide volume (Brien and Reid 2007, 2008). As GIS-based models of slope stability continue to improve and become integrated with models for debris flow and debris avalanche runout (Schilling 1998; Griswold and Iverson 2008), they can contribute to better estimates of downslope areas potentially impacted by landslides. Recent and ongoing research to improve models for predicting or mapping soil or colluvial depth is also expected to contribute to more accurate assessments of shallow landslide hazard (Dietrich et al. 1995; Roering 2008; Schulz et al. 2008; Pelletier and Rasmussen 2009; Catani et al. 2010; Ho et al. 2012). Ongoing work in model parameterization using sensitivity and probabilistic approaches combined with analysis of one or more historical landslide events is showing promise as a way to calibrate deterministic models (Gioia et al. 2013; Raia et al. 2013). These developments can make deterministic models useful in a wider range of settings, because even in many highly developed countries, few relevant data are available for most areas and spatial distribution of important factors is rarely known in sufficient detail.

Data and model uncertainty will always exist even as models improve and technological advancements make it possible to reduce uncertainty in certain types of spatial data. Nevertheless, if the current momentum of technological advancement and landslide hazard research continues unabated throughout the next decade, we can look forward to considerable progress in understanding and modeling where, when, and how often landslides are likely to occur. We can also expect advances in predicting their volumes and extents and being able to apply that knowledge to regional assessments of landslide hazard.

Acknowledgments Jeff Coe and Kevin Schmidt (both USGS) provided constructive reviews of the manuscript.

Disclaimer Any use of trade, product, or firm names in this publication is for descriptive purposes only and does not imply endorsement by the U.S. Government.

References

Aleotti P, Chowdury R (1999) Landslide hazard assessment: summary review and new perspectives. Bull Eng Geol Env 58:21–44

Artim ER (1976) Slope stability map of Thurston County, Washington. Geologic Map GM-15, Division of Geology and Earth Resources, Washington Department of Natural Resources, Olympia, WA, USA, 1:125,000

Baum RL, Coe JA, Godt JW, Harp EL, Reid ME, Savage WZ, Schulz WH, Brien DL, Chleborad AF, McKenna JP, Michael JA (2005) Regional landslide-hazard assessment for Seattle, Washington, USA. Landslides 2(4):266–279. doi:10.1007/s10346-005-0023-y

Baum RL, Savage WZ, Godt JW (2008) TRIGRS—A FORTRAN program for transient rainfall infiltration and grid-based regional slope-stability analysis, version 2.0. US Geological Survey Open-File Rep 2008-1159. http://pubs.er.usgs.gov/publication/ofr20081159

Baum RL, Godt JW, Savage WZ (2010) Estimating the timing and location of shallow rainfall-induced landslides using a model for transient, unsaturated infiltration. J Geophys Res 115:F03013. doi:10.1029/2009JF001321

Baum RL, Godt JW, Coe JA, Reid ME (2012) Assessment of shallow landslide potential using 1-D and 3-D slope stability analysis. In: Eberhardt E, Froese C, Turner AK, Leroueil S (eds) Landslides and engineered slopes: protecting society through improved understanding. Taylor & Francis, London, pp 1667–1672

Berti M, Simoni A (2007) Prediction of debris flow inundation areas using empirical mobility relationships. Geomorphology 90 (1–2):144–161

Borga M, Fontana GD, Ros DD, Marchi L (1998) Shallow landslide hazard assessment using a physically based model and digital elevation data. Environ Geol 35(2–3):81–88. doi:10.1007/s002540050295

Brabb EE, Pampeyan EH, Bonilla MG (1972) Landslide susceptibility in San Mateo County, California. US Geological Survey Miscellaneous Field Studies Map 360, 1:24,000

Brien DL, Reid ME (2007) Modeling 3-D slope stability of coastal bluffs using 3-D ground-water flow, southwestern Seattle, Washington. US Geological Survey Scientific Investigations Report 2007-5092. http://pubs.usgs.gov/sir/2007/5092/

Brien DL, Reid ME (2008) Assessing deep-seated landslide susceptibility using 3-D groundwater and slope-stability analyses, southwestern Seattle, Washington. In: Baum RL, Godt JW, Highland LM (eds) Engineering geology and landslides of the Seattle, Washington, area, vol 20, Geological Society of America reviews in engineering geology. Geological Society of America, Boulder, pp 83–101. doi:10.1130/2008.4020(05)

Burns WJ (2007) Comparison of remote sensing data-sets for the establishment of a landslide mapping protocol in Oregon. Conference presentations, 1st North American landslide conference, AEG Special Publication 23, Vail, CO

Burns WJ, Madin IP (2009) Protocol for inventory mapping of landslide deposits from light detection and ranging (LiDAR) imagery. Oregon Department of Geology and Mineral Industries Special Paper 42

Burns WJ, Madin IP, Mickelson KA (2012) Protocol for shallow landslide susceptibility mapping. Oregon Department of Geology and Mineral Industries Special Paper 45

Cannon SH, Gartner JE, Rupert MG, Michael JA, Rea AH, Parrett C (2010) Predicting the probability and volume of postwildfire debris flows in the intermountain western United States. Bull Geol Soc Am 122(1–2):127–144

Carrara A (1983) Multivariate models for landslide hazard evaluation. Math Geol 15(3):403–426

Carrara A, Cardinali M, Detti R, Guzzetti F, Pasqui V, Reichenbach P (1991) GIS techniques and statistical models in evaluating landslide hazard. Earth Surf Process Landforms 16:427–445

Carrara A, Guzzetti F, Cardinali M, Reichenbach P (1999) Use of GIS technology in the prediction and monitoring of landslide hazard. Nat Hazards 20:117–135. doi:10.1023/A:1008097111310

Catani F, Segoni S, Falorni G (2010) An empirical geomorphology-based approach to the spatial prediction of soil thickness at catchment scale. Water Resour Res 46, W05508. doi:10.1029/2008WR007450

Chung CF, Fabbri AG (2003) Validation of spatial prediction models for landslide hazard mapping. Nat Hazards 30:451–472. doi:10.1023/B:NHAZ.0000007172.62651.2b

Chung CJ, Fabbri A, van Westen CJ (1995) Multivariate regression analysis for landslide hazard zonation. In: Carrara A, Guzetti F (eds) Geographical information systems in assessing natural hazards. Kluwer Publications, Dordrecht, pp 107–133

Coe JA, Michael JA, Crovelli RA, Savage WZ, Laprade WT, Nashem WD (2004a) Probabilistic assessment of precipitation-triggered landslides using historical records of landslide occurrence, Seattle, Washington. Environ Eng Geosci 10(2):103–122

Coe JA, Godt JW, Baum RL, Bucknam RC, Michael JA (2004b) Landslide susceptibility from topography in Guatemala. In: Lacerda WA et al (eds) Landslides, evaluation and stabilization. Proceedings of the 9th international symposium on landslides, vol 1. Rio de Janeiro, pp 69–79

Crosta GB, Frattini R (2003) Distributed modeling of shallow landslides triggered by intense rainfall. Nat Hazards Earth Syst Sci 3:81–93

Dai FC, Lee CF (2003) A spatiotemporal probabilistic modelling of storm induced shallow landsliding using aerial photographs and logistic regression. Earth Surf Process Landforms 28(5):527–545

Dai FC, Lee CF, Ngai YY (2002) Landslide risk assessment and management: an overview. Eng Geol 64(1):65–87

Dietrich WE, Reiss R, Hsu M-L, Montgomery DR (1995) A process-based model for colluvial soil depth and shallow landsliding using digital elevation data. Hydrol Process 9:383–400. doi:10.1002/hyp.3360090311

Ellen SD, Mark RK, Cannon SH, Knifong DL (1993) Map of debris-flow hazard in the Honolulu District of Oahu, Hawaii. US Geological Survey Open-File Report, pp 93–213, 1:30,000

Falaschi F, Giacomelli F, Federici PR, Puccinelli A, D'Amato Avanzi G, Pochini A, Ribolini A (2009) Logistic regression versus artificial neural networks: landslide susceptibility evaluation in a sample area of the Serchio River valley, Italy. Nat Hazards 50:551–569. doi:10.1007/s11069-009-9356-5

Fawcett T (2006) An introduction to ROC analysis. Pattern Recognit Lett 27:861–874

Felicísimo ÁM, Cuartero A, Remondo J, Quirós E (2013) Mapping landslide susceptibility with logistic regression, multiple adaptive regression splines, classification and regression trees, and maximum entropy methods: a comparative study. Landslides 10(2):175–189

Franciss FO (2004) Landslide hazard assessment on hilly terrain. In: Lacerda WA, Ehrlich M, Fontoura SAB, Sayão ASF (eds) Landslides—evaluation and stabilization. Proceedings of the 9th international symposium on landslides, vol 1. Balkema, Rio de Janeiro, Brazil, pp 143–150

Frattini P, Crosta GB, Fusi N, Dal Negro P (2004) Shallow landslides in pyroclastic soils, a distributed modeling approach for hazard assessment. Eng Geol 73(3–4):277–295. doi:10.1016/j.enggeo.2004.01.009

Gioia E, Speranza G, Ferretti M, Marincioni F, Godt JW, Baum RL (2013) Rainfall induced shallow landslide forecasting in large areas: application of the TRIGRS model over a broad area of post-orogenic Quaternary sediments (Abstract). Geol Soc Am Abs Prog 45(7):775

Godt JW, McKenna JP (2008) Numerical modeling of rainfall thresholds for shallow landsliding in the Seattle, Washington, area. In: Baum RL, Godt JW, Highland LM (eds) Engineering geology and landslides of the Seattle, Washington, area, vol 20, Geological Society of America reviews in engineering geology. Geological Society of America, Boulder, CO, pp 121–135. doi:10.1130/2008.4020(07)

Godt JW, Schulz WH, Baum RL, Savage WZ (2008a) Modeling rainfall conditions for shallow landsliding in Seattle, Washington. In: Baum RL, Godt JW, Highland LM (eds) Engineering geology and landslides of the Seattle, Washington, area, vol 20, Geological Society of America reviews in engineering geology. Geological Society of America, Boulder, pp 137–152. doi:10.1130/2008.4020(08)

Godt JW, Baum RL, Savage WZ, Salciarini D, Schulz WH, Harp EL (2008b) Transient deterministic shallow landslide modeling: requirements for susceptibility and hazard assessments in a GIS framework. Eng Geol 102:214–226. doi:10.1016/j.enggeo.2008.03.019

Godt JW, Coe JA, Baum RL, Highland LM, Keaton JR, Roth RJ Jr (2012) Prototype landslide hazard map of the conterminous United States. In: Eberhardt E, Froese C, Turner AK, Leroueil S (eds) Landslides and engineered slopes: protecting society through improved understanding. Taylor & Francis Group, London, pp 245–250

Griswold JP, Iverson RM (2008) Mobility statistics and automated hazard mapping for debris flows and rock avalanches. US Geological Survey Scientific Investigations Report: 2007-5276

Guzzetti F, Carrara A, Cardinali M, Reichenbach P (1999) Landslide hazard evaluation: a review of current techniques and their application in a multi-scale study, Central Italy. Geomorphology 31(1–4):181–216. doi:10.1016/S0169-555X(99)00078-1

Haneberg WC (2008) Elevation errors in a LiDAR digital elevation model of West Seattle and their effects on slope stability calculations. In: Baum RL, Godt JW, Highland LM (eds) Engineering geology and landslides of the Seattle, Washington, area, vol 20, Geological Society of America reviews in engineering geology. Geological Society of America, Boulder, CO, pp 55–65. doi:10.1130/2008.4020(03)

Harbaugh AW, Banta ER, Hill MC, McDonald MG (2000) MODFLOW-2000, the US Geological Survey modular ground-water model—user guide to modularization concepts and the ground-water flow process. US Geological Survey Open-File Report 00-92

Harp EL, Noble MA (1993) An engineering rock classification to evaluate seismic rock-fall susceptibility and its application to the Wasatch Front. Bull Assoc Eng Geol 30:293–319

Harp EL, Michael JA, Laprade WT (2006) Shallow-landslide hazard map of Seattle, Washington. US Geological Survey Open-File Report 2006-1139. http://pubs.usgs.gov/of/2006/1139/

Harp EL, Michael JA, Laprade WT (2008) Shallow landslide hazard map of Seattle, Washington. In: Baum RL, Godt JW, Highland LM (eds) Engineering geology and landslides of the Seattle, Washington, area, vol 20, Geological Society of America reviews in engineering geology. Geological Society of America, Boulder, CO, pp 67–82. doi:10.1130/2008.4020(04)

Harp EL, Reid ME, McKenna JP, Michael JA (2009) Mapping of hazard from rainfall-triggered landslides in developing countries: examples from Honduras and Micronesia. Eng Geol 104:295–311

Harp EL, Keefer DK, Sato HP, Yagi H (2011) Landslide inventories: the essential part of seismic landslide hazard analyses. Eng Geol. doi:10.1016/j.enggeo.2010.06.013

Harp EL, Hartzell SH, Jibson RW, Ramirez-Guzman L (2012) Relation of landslides triggered by the Kiholo Bay earthquake and modeled ground motion. In: Eberhardt E, Froese C, Turner AK, Leroueil S (eds) Landslides and engineered slopes: protecting society through improved understanding. CRC, London, pp 507–510

Ho J-Y, Lee KT, Chang TC, Wang Z-Y, Liao Y-H (2012) Influences of spatial distribution of soil thickness on shallow landslide prediction. Eng Geol 124:38–46

Jibson RW, Harp EL, Michael JA (2000) A method for producing digital probabilistic seismic landslide hazard maps. Eng Geol 58:271–289

Kirschbaum DB, Adler R, Hong Y, Hill S, Lerner-Lam AL (2010) A global landslide catalog for hazard applications—method, results and limitations. Nat Hazards 52(3):561–575

Laprade WT, Kirkland TE, Nashem WD, Robertson CA (2000). Seattle landslide study. Shannon & Wilson, Inc. Internal Report W-7992 - 01. 164 pp. http://www.seattle.gov/dpd/cms/groups/pan/@pan/documents/web_informational/dpdp025740.pdf

Lee S, Ryu J-H, Min K, Won J-S (2003) Landslide susceptibility analysis using GIS and artificial neural network. Earth Surf Process Landforms 28(12):1361–1376

Lu P, Rosenbaum MS (2003) Artificial neural networks and grey systems for the prediction of slope stability. Nat Hazards 30 (3):383–398

Magirl CS, Griffiths PG, Webb RH (2010) Analyzing debris flows with the statistically calibrated empirical model LAHARZ in southeastern Arizona, USA. Geomorphology 119:111–124

Miller RD (1973) Map showing relative slope stability in part of west-central King County, Washington. US Geological Survey Miscellaneous Investigations Series Map, I-852-A, 1:48,000

Miller DJ (1995) Coupling GIS with physical models to assess deep-seated landslide hazards. Environ Eng Geosci 1(3):263–276

Montgomery DR, Dietrich WE (1994) A physically based model for the topographic control on shallow landsliding. Water Resour Res 30 (4):1153–1171. doi:10.1029/93WR02979

Montgomery DR, Sullivan K, Greenberg HM (1998) Regional test of a model for shallow landsliding. Hydrol Process 12(6):943–955. doi:10.1002/(SICI)1099-1085(199805)12:6,943:AID-HYP664.3.0.CO;2-Z

Ohlmacher GC, Davis JC (2003) Using multiple logistic regression and GIS technology to predict landslide hazard in northeast Kansas, USA. Eng Geol 69(3–4):331–343

Pack RT, Tarboton DG, Goodwin CN (1998) The SINMAP approach to terrain stability mapping. In: Proceedings of the 8th international congress of the international association of engineering geology and the environment, Vancouver, British Columbia, Canada, September 21–25, vol 2. AA Balkema, Rotterdam, pp 1157–1165

Pelletier JD, Rasmussen C (2009) Geomorphically based predictive mapping of soil thickness in upland watersheds. Water Resour Res 45, W09417. doi:10.1029/2008WR007319

Petley D (2012) Global patterns of loss of life from landslides. Geology 40(10):927–930

Raia S, Alvioli M, Rossi M, Baum RL, Godt JW, Guzzetti F (2013) Improving predictive power of physically based rainfall-induced shallow landslide models: A probabilistic approach. Geosci Model Dev Discuss 6:1367–1426. doi:10.5194/gmdd-6-1367-2013

Reid ME, Christian SB, Brien DL (2000) Gravitational stability of three-dimensional stratovolcano edifices. J Geophys Res 105 (B3):6043–6056. doi:10.1029/1999JB900310

Reid ME, Sisson TW, Brien DL (2001) Volcano collapse promoted by hydrothermal alteration and edifice shape, Mount Rainier, Washington. Geology 29(9):779–782

Reid ME, Brien DL, Waythomas CF (2010) Preliminary slope-stability analysis of Augustine Volcano. In: Power JA, Coombs ML, Freymueller JT (eds) The 2006 Eruption of Augustine Volcano, Alaska, US Geological Survey Professional Paper 1769, pp 321–332. http://pubs.usgs.gov/pp/1769/chapters/p1769_chapter14.pdf

Roering JJ (2008) How well can hillslope evolution models "explain" topography? Simulating soil transport and production with high-resolution topographic data. Geol Soc Am Bull 120(9/10):1248–1262. doi:10.1130/B26283.1

Roering JJ, Stimely LL, Mackey BH, Schmidt DA (2009) Using DInSAR, airborne LiDAR, and archival air photos to quantify landsliding and sediment transport. Geophys Res Lett 36(19). doi:10.1029/2009GL040374

Salciarini D, Godt JW, Savage WZ, Baum RL, Conversini P (2008) Modeling landslide recurrence in Seattle, Washington, USA. Eng Geol 102(3–4):227–237. doi:10.1016/j. enggeo.2008.03.013

Savage WZ, Godt JW, Baum RL (2003) A model for spatially and temporally distributed shallow landslide initiation by rainfall infiltration. In: Rickenmann D, Chen C (eds) Debris-flow hazards mitigation: mechanics, prediction, and assessment. Mill Press, Rotterdam, pp 179–187

Savage WZ, Godt JW, Baum RL (2004) Modeling time-dependent aerial slope stability. In: Lacerda WA, Erlich M, Fontoura SAB, Sayao ASF (eds) Landslides—evaluation and stabilization. Proceedings of the 9th international symposium on landslides, vol 1. Balkema, London, pp 23–36

Schilling S P (1998) LAHARZ; GIS programs for automated mapping of lahar-inundation hazard zones. US Geological Survey Open-File Report 98-638

Schulz WH (2004) Landslides mapped using LiDAR imagery, Seattle, Washington. US Geological Survey Open-File Report 2004-1396

Schulz WH (2007) Landslide hazards revealed by LiDAR imagery, Seattle, Washington. Eng Geol 89(1–2):67–87

Schulz WH, Lidke DJ, Godt JW (2008) Modeling the spatial distribution of landslide-prone colluvium and shallow groundwater on hillslopes of Seattle, WA. Earth Surf Process Landforms 33:123–141

Simoni S, Zanotti F, Bertoldi G, Rigon R (2008) Modelling the probability of occurrence of shallow landslides and channelized debris flows using GEOtop-FS. Hydrol Process 22(4):532–545. doi:10.1002/hyp.6886

Soeters R, van Westen CJ (1996) Slope instability recognition, analysis, and zonation. In: Turner AK, Schuster RL (eds) Landslides, investigation and mitigation. Transportation Research Board Special Report 247. National Research Council, Washington, DC, pp 129–177

Suzen ML, Doyuran V (2003) A comparison of the GIS based landslide susceptibility assessment methods: multivariate versus bivariate. Environ Geol. doi:10.1007/s00254-003-0917-8

Swets J (1988) Measuring the accuracy of diagnostic systems. Science 240:1285–1293

Troost KG, Booth DB, Wisher AP, Shimel SA (2005) The geologic map of Seattle–A progress report. US Geological Survey Open-file Report 2005-1252

van Beek LPH, van Asch TWJ (2004) Regional assessment of the effects of land-use change on landslide hazard by means of physically based modeling. Nat Hazards 31:289–304

Van den Eeckhaut M, Vanwalleghem T, Poesen J, Govers G, Verstraeten G, Vandekerckhove L (2006) Prediction of landslide susceptibility using rare events logistic regression: a case-study in the Flemish Ardennes (Belgium). Geomorphology 76:392–410

van Westen CJ, Terlien MTJ (1996) An approach towards deterministic landslide hazard analysis in GIS: a case study from Manizales (Colombia). Earth Surf Process Landforms 21(9):853–868

van Westen CJ, Rengers N, Soeters R (2003) Use of geomorphological information in indirect landslide susceptibility assessment. Nat Hazards 30(3):399–419

van Westen CJ, van Asch TWJ, Soeters R (2006) Landslide hazard and risk zonation—why is it still so difficult? Bull Eng Geol Env 65:167–184. doi:10.1007/s10064-005-0023-0

Varnes DJ (1981) The principles and practice of landslide hazard zonation. Bull Int Assoc Eng Geol 23:13–14

Varnes DJ (1984) Landslide hazard zonation: a review of principles and practice. UNESCO, Paris, 60 pp

Wait TC (2001) Characteristics of deep-seated landslides in Seattle, Washington. M.S. thesis, Colorado School of Mines, Golden, CO

Wu W, Sidle RC (1995) A distributed slope stability model for steep forested hillslopes. Water Resour Res 31:2097–2110

Xie M, Esaki T, Zhou G (2004) GIS-based probabilistic mapping of landslide lazard using a three-dimensional deterministic odel. Nat Hazards 33:265–282